Time-resolved double-resonance spectroscopy: Lifetime measurement of the $6\,^1\Sigma_g^+(7,31)$ electronic state of molecular sodium

Michael Saaranen,[1] Dinesh Wagle,[1] Emma McLaughlin,[2] Amelia Paladino,[2] Seth Ashman,[2] and S. Burçin Bayram[1,a)]

[1]*Department of Physics, Miami University, Oxford, Ohio 45056, USA*
[2]*Department of Engineering, Physics, and Systems, Providence College, Providence, Rhode Island 02918, USA*

We report on the lifetime measurement of the $6\,^1\Sigma_g^+(7,31)$ state of Na$_2$ molecules, produced in a heat-pipe oven, using a time-resolved spectroscopic technique. The $6\,^1\Sigma_g^+(7,31)$ level was populated by two-step two-color double resonance excitation via the intermediate $A\,^1\Sigma_u^+(8,30)$ state. The excitation scheme was done using two synchronized pulsed dye lasers pumped by a Nd:YAG laser operating at the second harmonics. The fluorescence emitted upon decay to the final state was measured using a time-correlated photon counting technique, as a function of argon pressure. From this, the radiative lifetime was extracted by extrapolating the plot to collision-free zero pressure. We also report the calculated radiative lifetimes of the Na$_2$ $6\,^1\Sigma_g^+$ ro-vibrational levels in the range of $v = 0$–200 with $J = 1$ and $J = 31$ using the LEVEL program for bound-bound and the BCONT program for bound-free transitions. Our calculations reveal the importance of the bound-free transitions on the lifetime calculations and a large difference of about a factor of three between the $J = 1$ and $J = 31$ for the $v = 40$ and $v = 100$, respectively, due to the wavefunction alternating between having predominantly inner and outer well amplitude. *Published by AIP Publishing.* https://doi.org/10.1063/1.5061729

I. INTRODUCTION

Alkali diatomic molecules have been widely studied by theoreticians and experimentalists for many years due to their simple and rich internal structures. Investigations of the molecular structure and dynamics of short-range potentials and photodissociation, predissociation, autoionization, and energy transfer processes using traditional short-range molecular spectroscopy are important for ultracold physics. In recent years, cold and ultracold (bi)alkali diatomic molecules have been at the forefront of quantum chemistry and many-body physics. These molecules have been used to probe new states of quantum matter, to improve precision measurements of fundamental constants, and in the development of quantum information storage and molecule lasers.[1–8] While the radiative properties of ultracold molecules are no longer restricted by collisional de-excitation, preparing dense samples of ultracold diatomic molecules in a specific quantum state still remains challenging. This work deals with the experimental and theoretical studies of the $6\,^1\Sigma_g^+(3s + 5s)$ state in sodium diatomic molecules. The sodium dimer exhibits an exotic behavior of the $6\,^1\Sigma_g^+$ symmetry with double well (inner and outer) structures due to the sodium positive and negative ion pair potential energy interaction. The existence of an outer-well ($8a_o < R < 40a_o$) of this potential curve may play an important role for the production of cold ground state molecules.

The potential curves of electronic states up to the Na$_2$ $(3s + 5s)$ dissociation limit for the singlet and triplet electronic states and radiative lifetimes of a band of vibrational levels for various electronic states have been studied using various methods.[9–16] Recent experimental and theoretical studies of the radiative lifetimes of the $2\,^1\Sigma_u^+$ state of sodium dimers have been reported using a molecular beam apparatus and pulsed dye lasers with a pump-delayed probe technique by Anunciado *et al.*[16] The authors demonstrated for the first time the importance of the inclusion of the bound-free transitions into the lifetime calculations. Despite considerable interest in the electronic states of sodium diatomic molecules, the radiative lifetimes of the $6\,^1\Sigma_g^+$ inner-well state have not been measured by experimentalists. The lifetimes of the outer-well of this state have been reported in a multi-step laser excitation method.[17] In this paper, we report for the first time lifetime measurements of the inner-well of the $6\,^1\Sigma_g^+(7,31)$ state using a time-correlated photon counting technique and theoretical calculations in various ro-vibrational levels of the $6\,^1\Sigma_g^+$ state using bound-bound and bound-free transitions. We also demonstrate the effect of inclusion of the bound-free transitions in the calculated radiative lifetime of the $6\,^1\Sigma_g^+$ $(3s + 5s)$ ro-vibrational levels in the range of $v = 0$–200 with $J = 1$ and $J = 31$. We report the transition dipole moment functions coupling the $6\,^1\Sigma_g^+$ state to seven electronic states with singlet, ungerade symmetry and also the branching ratios for radiative transitions from the $6\,^1\Sigma_g^+$ ro-vibrational levels into those seven states. We discuss the results of both experimental and theoretical lifetimes of the $6\,^1\Sigma_g^+$ $(3s + 5s)$ state.

a)Electronic mail: bayramsb@MiamiOH.edu

The remainder of this paper is organized as follows: Sec. II contains a description of the experimental apparatus including the excitation scheme and potential energy curves of Na$_2$, Sec. III presents new measurements including the techniques used, Sec. IV describes the theoretical calculations, followed by results and discussion in Sec. V, and conclusion in Sec. VI.

II. EXPERIMENT

The time-resolved double-resonance experimental setup is shown in Fig. 1. The sodium metal is contained in a 4-arm crossed heat-pipe oven.[18–21] The desired amount of buffer gas was introduced into the heat-pipe when the oven was cold and the background pressure was about 15 mTorr. The gas valve was closed to keep a fixed amount of argon gas inside the oven. The oven, which has a length of 1 m, is then heated by eight non-magnetic ceramic heaters to produce sodium vapor, while cold water is run through copper coils wrapped near the windows of the arms. The heat-pipe oven and the ceramic heaters were wrapped with a ceramic fiber blanket to maintain a homogenous temperature inside the oven. A stainless steel mesh lining the arms of the oven walls acts as a wick to return the liquid metal back to the central region of the oven in order to prevent condensation onto the windows. During the experiment, argon pressure was continuously monitored by using an absolute capacitance manometer (MKS 627E), temperature-controlled to 45 °C. To create sodium molecules, the heat-pipe is heated to 290 °C and the temperature of the central region of the oven was monitored with a thermocouple probe. At the operating temperature of 290 °C, about 32.6% of the molecules are in the vibrational ground state $v'' = 0$, 21.8% in $v'' = 1$, 14.6% in $v'' = 2$, 9.85% in $v'' = 3$, ..., 1.45% in $v'' = 8$ and less than 1 in levels $v'' = 9$ and higher. The Nesmeyanov vapor pressure formula is used to estimate the sodium molecular and atomic vapor densities at the operating temperature of the heat-pipe oven,[22] yielding a number
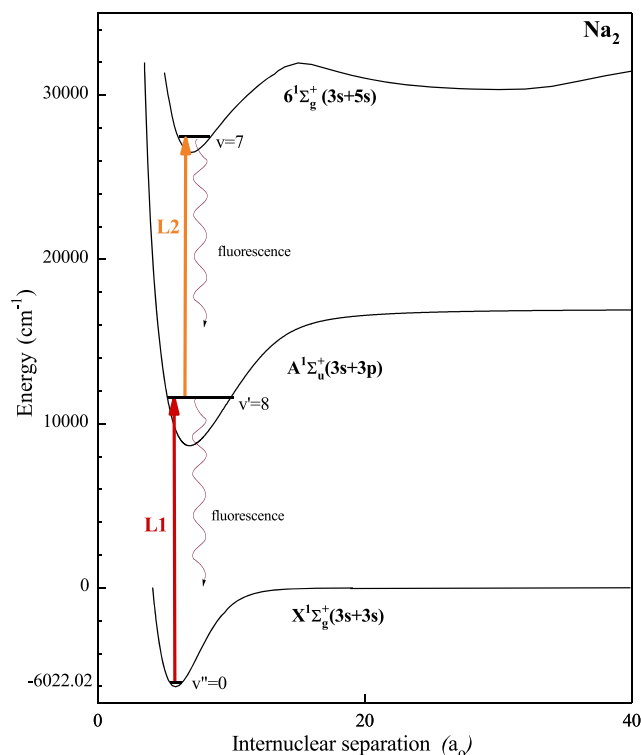

FIG. 2. Experimental excitation to the $6\,^1\Sigma_g^+(3s + 5s)$ state and the detection scheme on a partial energy level diagram of Na$_2$.

density at 290 °C for the sodium dimers of 1.45×10^{12} cm^{-3} and for the sodium atoms of 7.35×10^{14} cm^{-3}.

The partial energy level diagram of Na$_2$ and the experimental excitation scheme are shown in Fig. 2. The excitation lasers are tunable home-built pulse dye lasers whose cavity designs are of the grazing incidence Littman-Metcalf[23] type. Both dye lasers operate in a single transverse mode and are pumped by the second harmonics (532 nm) of a
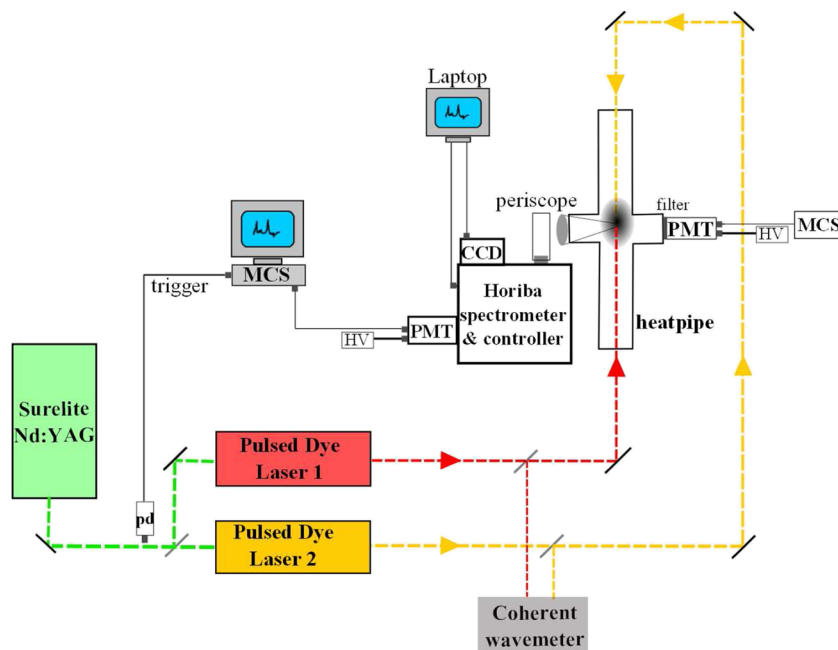

FIG. 1. A schematic view of the experimental setup. The tunable dye lasers are pumped by the pulse Nd:YAG laser. The slit widths and swing-away mirror of the spectrometer are computer-controlled. The CCD is a charge-couple device, cooled to −40 °C, with 14×10^{-6} m pixel size. MCS is a multi-channel scaler for time-correlated photon counting, PMT refers to a photomultiplier tube, pd refers to a photodiode, and a periscope, consisting of two mirrors, is used to invert the horizontal image to vertical in order to optimize the fluorescence collection at the entrance slit of the Horiba spectrometer.

Nd:YAG laser with a pulse repetition rate of 20 Hz. They produce about 0.5 mW average power with bandwidths less than 6 GHz (≤ 0.2 cm^{-1}). Dye laser 1, L1, drives the $X\,^1\Sigma_g^+(0, 29)$ $\rightarrow$ $A\,^1\Sigma_u^+(8, 30)$ transition at 15 518.5 cm^{-1} (644 nm), while the second dye laser, L2, drives the $A\,^1\Sigma_u^+(8, 30)$ $\rightarrow$ $6\,^1\Sigma_g^+(7, 31)$ transition at 17 798.9 cm^{-1} (561.8 nm). Laser wavelengths are measured using a Coherent wavemeter with a precision of 0.01 cm^{-1}. The lasers, both collimated to a 1-cm beam diameter, collinearly counterpropagate in the interaction region of the heat-pipe oven. The pulse duration of the lasers, about 6 ns, was measured using an ultrafast phototube with 270 ps risetime and 100 ps fall time. The L2 pulse arrives at the interaction region of the oven 4 ns after the arrival time of the L1 pulse. Due to the 2 ns temporal overlap time compared to the radiative lifetime of the excited level,[11] about 23% of the excited molecules will have radiatively decayed during the pulse. This overlap time sufficiently populates the $6\,^1\Sigma_g^+(7, 31)$ state. Molecular fluorescence emission from the $6\,^1\Sigma_g^+(7, 31)$ state is collected at the right angles to the propagation directions of the lasers using a periscope and an imaging spectrometer-detector system. The imaging spectrometer, Horiba iHR320, acts as a narrowband filter and has three built in diffraction gratings (600, 1200, and 2400 groves/mm), the 1200 g/mm is predominantly used throughout the experiment. The spectrometer has two exit ports (each port can be selected with a motorized swing away mirror): the front port has a back illuminated thermoelectrically cooled (-50 °C) charge-couple device (CCD) chip with 14×10^{-6} m squared pixel size, while the side port has a slit and a photomultiplier tube (PMT). The widths of the slits and swing away mirror are remotely controlled. The spectrometer is calibrated with a mercury light source. The FWHM resolution of the spectrometer, with the 1200 g/mm holographic grating (blazed at 500 nm) and the side slit at 90×10^{-6} m, is 19.33 cm^{-1} at 17 798.9 cm^{-1} and 14.19 cm^{-1} at 15 518.5 cm^{-1}. For lifetime measurements, the data were collected from the side slit (width at 90×10^{-6} m) using a PMT-multichannel scaler (MCS). A second photomultiplier tube (Hamamatsu R928), with an interference filter, was mounted on the second window of the heat-pipe and used to monitor the Na atomic fluorescence from the 4p state to the ground state.

III. MEASUREMENTS

With the setup shown in Fig. 1, a resolved molecular fluorescence spectrum was acquired from the $6\,^1\Sigma_g^+(7, 31)$ state as shown in Fig. 3. The spectrum exists only when the double-resonance excitation to the $6\,^1\Sigma_g^+(7, 31)$ state is accomplished. This detection scheme is almost background-free because the frequencies of this spectrum are far away from the molecular fluorescence from the $A\,^1\Sigma_u^+$ state, excited by Laser 1. In addition, it was not possible to observe any molecular fluorescence from the $6\,^1\Sigma_g^+(7, 31)$ state using Laser 1 or Laser 2 alone, and thus no two-photon absorption was observed from the $6\,^1\Sigma_g^+(7, 31)$ state. As a result, the spectrum suggests the two-step double-resonance for the $X\,^1\Sigma_g^+(0, 29)$ $\rightarrow$ $A\,^1\Sigma_u^+(8, 30)$ $\rightarrow$ $6\,^1\Sigma_g^+(7, 31)$ transition. The spectral peaks were identified by comparing them with the output of the LEVEL 8.0 Fortran program. This program uses experimental potential energy curves and calculates quantities such as Franck-Condon factors, Einstein coefficients, transition dipole moment matrix elements, and energies of the ro-vibrational levels. High Franck-Condon factors suggest that P- and R-branches from the $6\,^1\Sigma_g^+(v = 7, J = 31)$ to the $A\,^1\Sigma_u^+(v = 3 - 8, J = 30, 32)$ state should be readily observed and identified, and they are shown in Fig. 3. We report the lifetime measurements from the $v = 6$ doublet. The separation between the (6, 30) and (6, 32) doublet is 13.40 cm^{-1} according to the output of the LEVEL Fortran program. The photon counting technique is used to perform low-light-level
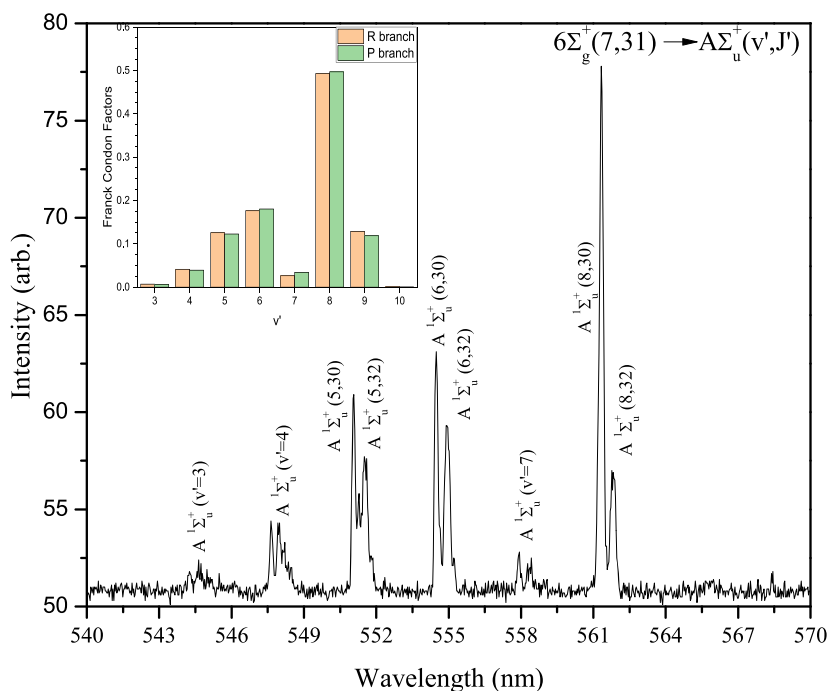

FIG. 3. Double-resonance spectrum from the $6\,^1\Sigma_g^+$ (7, 31) state. The spectrum, only obtained when both lasers are on resonance, was taken using a 1200 g/mm spectrometer-CCD with a FWHM resolution of 3 cm^{-1}. The spectral peaks mainly consist of $R(30)$, $P(32)$ doublets for the $A\,^1\Sigma_u^+(v', J')$ $\leftarrow$ $6\,^1\Sigma_g^+(7, 31)$ fluorescence emission, and they are identified by comparing to the output of the LEVEL 8.0 program. The inset shows the Franck-Condon factors, extracted from the program, as a function of vibrational quantum number.

measurement with high sensitivity and accuracy. There is a slight discrepancy between the resolved bound-bound spectrum and the computed Franck-Condon factors, with the exception of the transition associated with the upward laser transition, namely, $A\,^1\Sigma_u^+(8,30) \rightarrow 6\,^1\Sigma_g^+(7,31)$. The laser line is enhanced in the spectrum, and therefore the intensity of the downward fluorescence (8, 32) is likely lower than the intensity of the (8, 30) fluorescence. Therefore the calculations of the Franck-Condon factor to $v = 8$ (and $v = 9$ as well) are much larger than the spectrum suggests.

To do time-correlated photon counting, we used a multichannel scaler (MCS) which has a fast amplifier, a built-in discriminator, and 5-ns bin width (the temporal resolution). This technique is used to record low level light signals for the radiative lifetime measurements. The time accuracy is not limited by the width of the PMT detector pulse, and thus there is no loss due to gating as in Boxcar devices or gated CCDs. The MCS works by measuring the time between a trigger pulse and an associated PMT pulse which results from a single photon. We measure about one photon per five or more triggers. When the MCS receives a trigger pulse, a record of up to about 32 000 time bins, in our case about 1000 time bins of 5-ns, starts. During a record, when a signal pulse is received, one count is added to the time bin corresponding to when the pulse is received in relation to the trigger. The MCS was triggered by laser pulses from the YAG laser using a photodiode, and a scan of 20 000 records was accumulated and displayed on the screen on real-time. The resulting histogram yielded the fluorescence decay as a function of time. If the number of molecules leaving the $6\,^1\Sigma_g^+(v,J)$ state during the time interval dt is $N = -k_r N dt - k_{nr} N dt$, the solution gives the emitted radiation with intensity proportional to $N(t) = N_o e^{(k_r+k_{nr})t}$, where N_o is the initial population, k_r is the radiative decay, and k_{nr} is the non-radiative decay. Then, the lifetime is defined as $N(t)e^{-t/\tau_e}$. The typical result, a histogram with an exponential drop of counts as a function of time from the MCS, is shown in
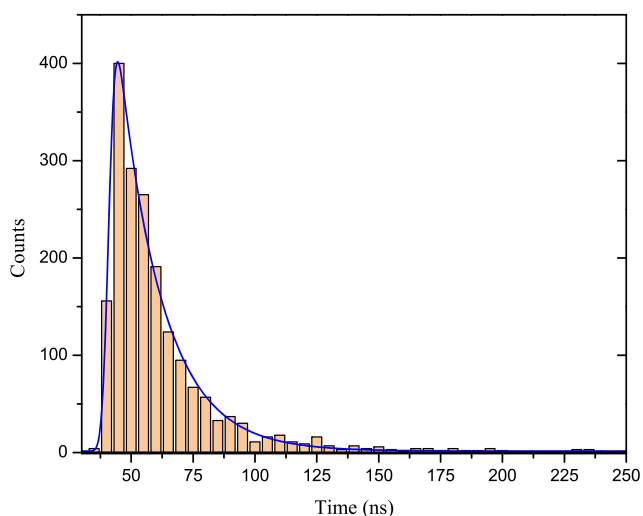
Fig. 4. The recorded data were transferred to a computer and the effective lifetime, τ_e, was obtained from the convolution of a Gaussian with an exponential fit to the data using Origin 2017. During the experiment, each scan was accumulated for 40 min to produce a full decay curve and more than ten independent measurements were done at one pressure point on various days. The average of the effective lifetime was calculated for each pressure setting. In order to determine the collision-free lifetime, this procedure was repeated at argon pressures ranging from 200 mTorr to 460 mTorr (at the operating temperature) and thus the effective lifetime as a function of pressure was obtained and plotted. A linear dependence of such a plot, known as Stern-Volmer, is expected if the probability of the multiple collisions is negligible. The Stern-Volmer relationship can be written as

$$\frac{1}{\tau_e} = \frac{1}{\tau_r} + \frac{1}{\tau_{nr}}, \qquad (1)$$

where τ_e is the effective lifetime, τ_r is the radiative lifetime, and $\tau_{nr}^{-1} = N_p \bar{v} \sigma$. Here, N_p is the number density of the buffer gas, $\bar{v}$ is the average velocities of the colliding Na_2^*–Ar atoms over the Maxwell-Boltzmann distribution of relative velocities at the heat-pipe oven temperature, and σ is the collisional cross section between the excited dimer and argon atoms. The approximate value for the number density of argon at the relevant pressure is on the order of 10^{16} cm^{-3}. Comparing this value to the sodium atomic and molecular densities, the argon density is at least two orders of magnitude larger. Thus, the contributions from sodium collisions are negligible. The effect of argon gas collisions is eliminated with the Stern-Volmer extrapolation. The radiative lifetime was extracted from the zero pressure extrapolation of the Stern-Volmer plot. Figure 5 shows the inverse lifetimes (ns) as a function of argon pressure at 290 °C in the range of 200 mTorr–450 mTorr. The radiative lifetime at the collision-free limit (intercept of the Stern-Volmer plot) was extracted from a linear fit to the data.

FIG. 4. A typical time-correlated photon counting scan (40 min to complete one decay curve) illustrating a histogram consisting of a range of "time bins" from the MCS. The blue line is a convolution fit of a Gaussian with an exponential curve function to the data with a correlation coefficient of 0.99. The effective lifetime of the molecular excited state was extracted from this convolution fit.
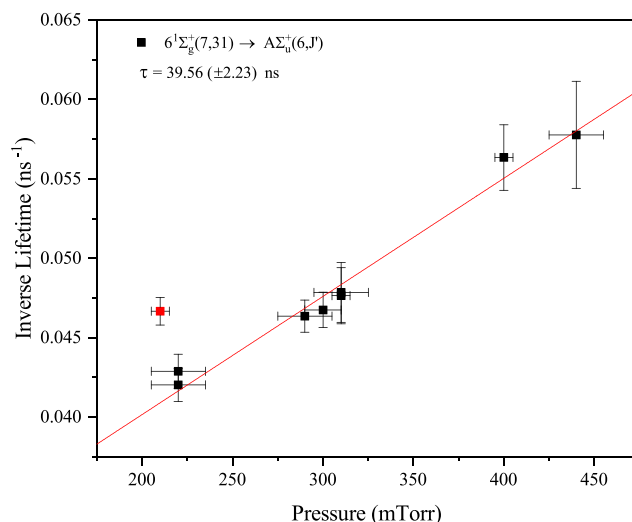

FIG. 5. Plot showing the variation in the inverse lifetime as a function of argon pressure at 290 °C. Each data point is an average of 10–20 independent lifetime measurements, with the error bar equal one standard deviation. Red filled square data point is an outlier and was excluded in the fitting procedure. Red line shows a weighted linear fit to the data with a correlation coefficient of $R^2 = 0.98$ and a residual sum square of 7.86×10^{-9}.

The radiative lifetime of the $6\,^1\Sigma_g^+(7,31)$ state is found to be 39.56 ($\pm$2.23) ns with a correlation coefficient of 0.99 and a residual sum square of 7.86×10^{-9}.

The effect of high pressure on the lifetime measurements was observed for pressures from about 500 mTorr to 1700 mTorr. A slight curving trend at high pressures may indicate the possibility of the buffer gas quenching effect[24] which can be studied in the future. For the purpose of determining the radiative lifetime at the collision-free limit, a linear fit to the data was done at low pressures. Additionally, we repeated the time-correlated photon counting experiments at different operating temperatures ranging from 290 °C to 340 °C and at different laser powers. The data showed no laser power dependency on lifetime measurements. However, as expected, lifetime decreased as we increased the temperature to 340 °C. To ensure the reproducibility of the data, we have repeated the experiments on different days. We have validated our measurements and setup by repeating the measurements for the known lifetimes of the Na_2 $A\,^1\Sigma_u^+(7,31)$ state under the same experimental conditions. The extracted radiative lifetime from the Stern-Volmer plot is found to be 14.02 (93) ns, comparable with the literature values of 13.11 (47) ns[10] and 12.51 (62) ns.[11]

In addition, we observed atomic fluorescence from the Na $4p\,^2P_J$ state to the $3s\,^2S_{1/2}$ ground state using a 330 nm interference filter. This is due to the molecular dissociation into the Na_2 (3s + 4p) asymptote. The signal exists only when molecules were formed in the heat-pipe. To ensure that the atomic fluorescence is not a result of an accidental dissociation into the Na_2 (3s + 5s) asymptote and then branching into the $4p$ state we monitored fluorescence for the $5s\,^2P_J \rightarrow 4p\,^2P_J$ transition at 615 nm and found no evidence.

IV. THEORETICAL CALCULATIONS

All lifetime calculations presented here were performed using the LEVEL 8.2 Fortran program, developed by Le Roy,[25] for the bound-bound transitions and the BCONT Fortran program for the bound-free transitions. The LEVEL code solves the radial Schrödinger equation of bound and quasi-bound levels with appropriate input for the transition dipole moment function[26] and relevant potential energy curves. The dipole selection rules allow spontaneous emission from the $6\,^1\Sigma_g^+(v,J)$[14,17] to seven electronic potentials: $1(A)\,^1\Sigma_u^+$ from Tiemann *et al.*,[27] $1(B)\,^1\Pi_u^+$ from Comacho *et al.*[28] and Tiemann,[29] $2\,^1\Sigma_u^+$ from Pashov *et al.*,[30] $2\,^1\Pi_u^+$ from Grochola *et al.*,[31] $3\,^1\Sigma_u^{+}$[32] and $3\,^1\Pi_u^+$ from Grochola *et al.*,[33] and $4\,^1\Sigma_u^+$ from Grochola *et al.*[34] The potentials and transition dipole moment functions for the seven dipole allowed transitions from the $6\,^1\Sigma_g^+(v,J)$ state are shown in Figs. 6 and 7, respectively.

The LEVEL 8.2 program computes the Einstein A coefficient for spontaneous emission, A_{if}, from an initial level $|i\rangle = |\alpha, v, J\rangle$ to a final level $|f\rangle = |\alpha', v', J'\rangle$. This coefficient can be expressed as[35,36]

$$A_{if} = \frac{16\pi^3}{3} \frac{k_{if}^3}{\epsilon_o h} \frac{S_{JJ'}}{(2J+1)} |\langle \psi_{v',J'}^{\alpha'}|M(r)|\psi_{v,J}^{\alpha}\rangle|^2, \quad (2)$$
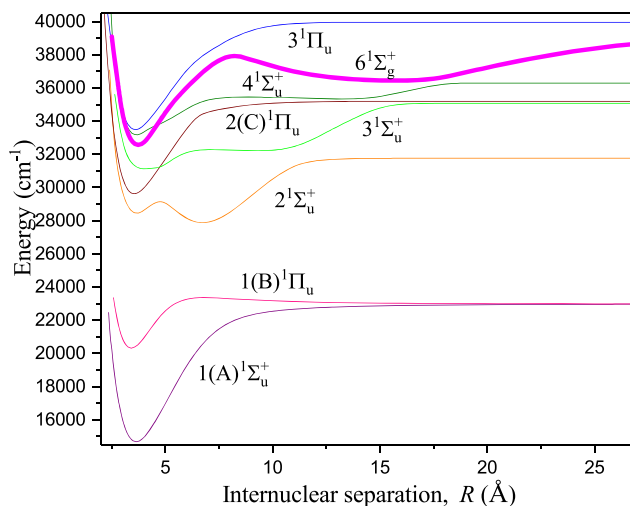

FIG. 6. Na_2 $6\,^1\Sigma_g^+$ potential energy function and the singlet, ungerade electronic states used in calculations into which excited molecules in the $6\,^1\Sigma_g^+$ state can decay.

where α denotes the electronic state, v and J are vibrational and rotational quantum numbers respectively, A_{if} has units s^{-1}, $M(r)$ is the transition dipole moment function, k_{if} is the emission wavenumber, $S_{JJ'}$ is the Hönl-London rotational intensity factor, $\psi_{v,J}^{\alpha}$ is the normalized radial nuclear wavefunctions belonging to initial and final states of the transition.

In cases where the sum of the Franck-Condon factors is less than one, we incorporated bound-free transitions using the BCONT code which computes the intensity as a function of wavelength. All bound-free calculations were completed using a modified version of the BCONT 2.2[37] program. The modifications have been described previously in Ref. 16 and even greater detail in Ref. 38 and therefore will not be repeated here. The bound-free calculations are more labor intensive than the bound-bound transitions, and therefore the ro-vibrational levels $6\,^1\Sigma_g^+(v = 0, 7, 8, 20, 40, 75, 100, 125, 155, 174, 200, J = 1, 31)$ were selected because they include energy levels with
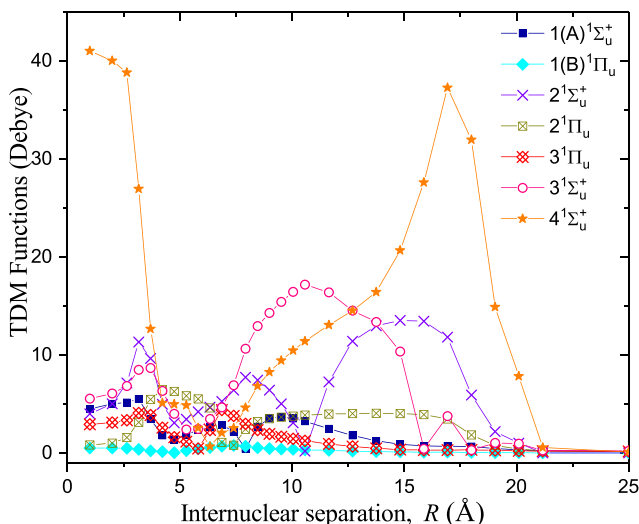

FIG. 7. Transition dipole moment (TDM) functions that couple the $6\,^1\Sigma_g^+$ state to each of the other potentials used in the calculations.
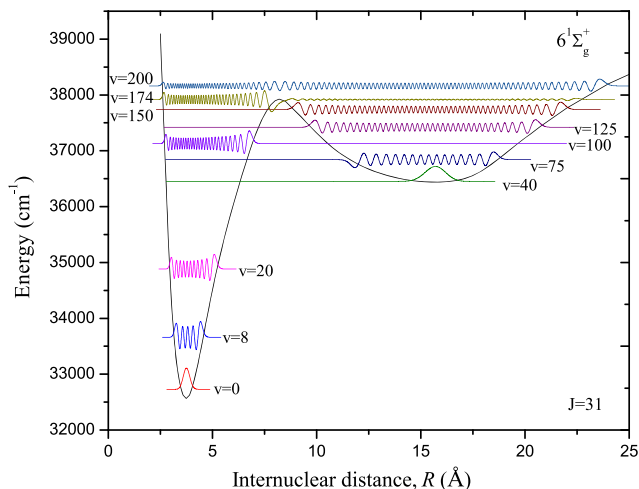
FIG. 8. $6\,^1\Sigma_g^+$ potential with the wavefunctions of the $v = 0, 8, 20, 40, 75, 100,$ 125, 155, 174, and 200, all with $J = 31$, plotted at the energy of their respective ro-vibrational level. Note that the wavefunctions existing in the region where two separated wells exist ($v = 40, 75, 100, 125, 155,$ and 174) do oscillate in both wells; however, all but $v = 174$ must be scaled up several orders of magnitude for those oscillations to become visible.

wavefunctions that reside in the inner well below the double well region, in the double minimum region, and in the region just above where the inner and outer well merge. Figure 8 shows some of the calculated wavefunctions used by the LEVEL and BCONT programs.

The revised BCONT code calculates the bound-free intensity dI per molecule emitted into a small energy band dE at photon energy $E = hck$ given by $dI = E \cdot \Gamma_{if}^{\alpha''} dE$, where the photon emission rate is given by

$$\Gamma_{if}^{\alpha'} dE = \frac{16\pi^3}{3} \frac{k_{if}^3}{\epsilon_o h} \frac{S_{JJ'}}{(2J+1)} |\langle \psi_{E',J'}^{\alpha'} | M(r) | \psi_{E,J}^{\alpha} \rangle|^2 dE. \quad (3)$$

The main difference between this photon emission rate and the bound-bound version in Eq. (2) is the replacement of the final state bound wavefunction $\psi_{v,J}^{\alpha}$ with the continuum wavefunction, $\psi_{E,J}^{\alpha}$. The lifetime of a single ro-vibrational level of the
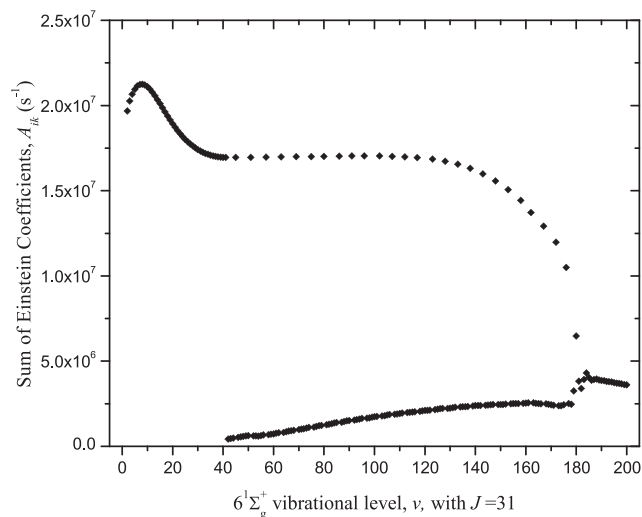

FIG. 9. Each point on this plot represents the sum of all Einstein coefficients originating from a single ro-vibrational level, $6\,^1\Sigma_g^+(v,J)$, to all bound levels of final state α'. In this plot, the final state is $\alpha' = 1(A)\,^1\Sigma_g^+$ and the vibrational levels $v = 0$–200 with $J = 31$ are shown. The upper branch is produced by $6\,^1\Sigma_g^+(v,J)$ levels with predominantly inner well wavefunctions, while the lower branch corresponds to those with predominantly outer well wavefunctions. Around approximately $v = 180$, the wavefunctions accrue substantial amplitude in both inner and outer regions as the two wells merge.

$6\,^1\Sigma_g^+$ is determined using the relation

$$\frac{1}{\tau_i} = \sum_{\alpha'} \left(\sum_f A_{if} + \int_0^{E(\alpha')} \Gamma_{if}^{\alpha'} dE \right), \quad (4)$$

where the A_{if} coefficients have been obtained from the LEVEL calculations, the $\Gamma_{if}^{\alpha'} dE$ from BCONT, and the overall sum includes all dipole allowed transitions. The bound-bound sum extends over all levels in the given electronic state α', and the integral extends from zero frequency to the appropriate threshold $E(\alpha') = E(v, J) - E(\alpha'$ asymptotic energy). The sum of Einstein coefficients as a function of $6\,^1\Sigma_g^+$ vibrational level for transitions to the $A\,^1\Sigma_u^+$ is plotted in Fig. 9. If the A_{if} and $\Gamma_{if}^{\alpha'} dE$ for a single final electronic state, α', are summed
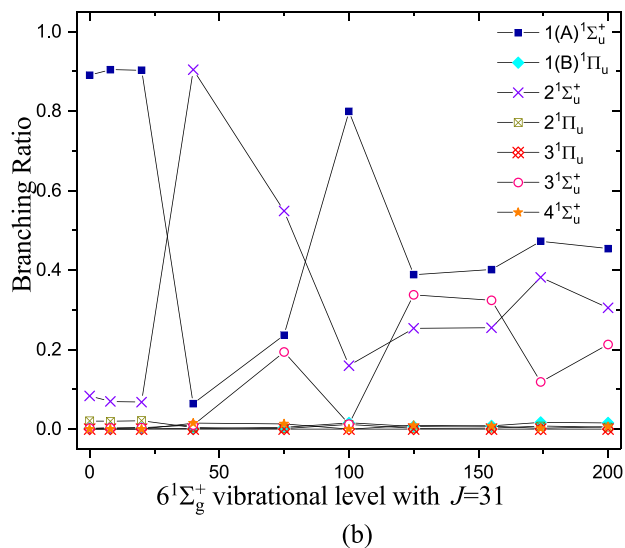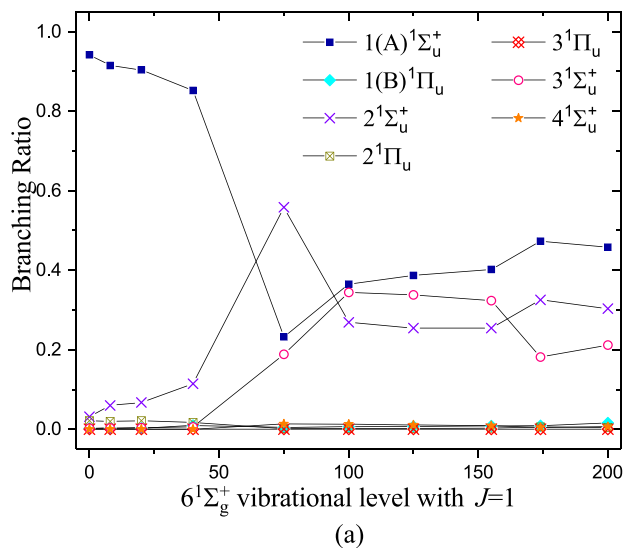

(a)

(b)

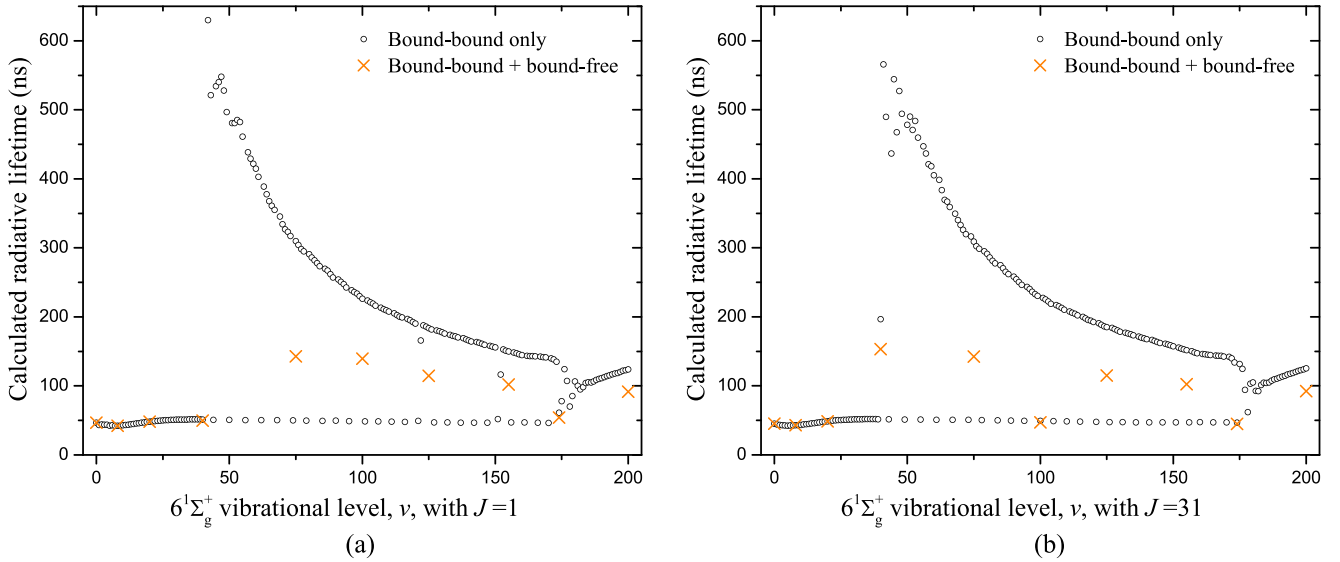FIG. 10. Branching ratios for $6\,^1\Sigma_g^+$ ro-vibrational levels with $J = 1$ and $J = 31$.

FIG. 11. Calculated lifetimes of $6\,^1\Sigma_g^+(v, J = 1, 31)$ ro-vibrational levels in the range $v = 0 - 200$. The upper branch is produced by ro-vibrational states with wavefunctions that have predominantly outer well amplitude, while the lower branch wavefunctions are predominantly the inner well. The open circles were computed using only bound-bound transitions, $\tau^{-1} = \sum_{\alpha'} \sum_f A_{if}^{\alpha'}$, while the orange X represents lifetimes calculated as in Eq. (4). The inclusion of bound-free transitions causes a much larger reduction of the calculated lifetimes for the ro-vibrational levels with appreciable outer well wavefunction amplitude since there is generally a less favorable overlap of the $6\,^1\Sigma_g^+$ outer well.

and divided by the full sum over all α' in Eq. (4), one obtains the branching ratio, r_b^α, into the final state α', i.e.,

$$r_b^a = \frac{\left(\sum_f A_{if} + \int_0^{E(\alpha')} \Gamma_{if}^{\alpha'} dE\right)}{\sum_{\alpha'}\left(\sum_f A_{if} + \int_0^{E(\alpha')} \Gamma_{if}^{\alpha'} dE\right)}. \quad (5)$$

Branching ratios for $J = 1$ and $J = 31$, for the calculations that include both bound-bound and bound-free transitions, are plotted in Fig. 10. Note that the rather small branching ratios for the $1(B)\,^1\Pi_u$, $2\,^1\Pi_u$, $3\,^1\Pi_u$, and $4\,^1\Sigma_u^+$ states indicate that they have minimal impact on the resulting lifetimes since the excited molecule has a lower probability of decaying through

those states. Conversely, the $1(A)\,^1\Sigma_u^+$, $2\,^1\Sigma_u^+$, and $3\,^1\Sigma_u^+$ states offer the most probable decay paths for the excited molecule.

Figure 11 shows our calculated radiative lifetimes of the $6\,^1\Sigma_g^+$ ro-vibrational levels in the range of $v = 0$–200 with $J = 1$ and $J = 31$. This figure clearly demonstrates the importance of the bound-free transitions in the calculations. A strong dependence of the calculated radiative lifetime on the radial coordinate, R, is observed, causing two distinct branches to occur in the portion of the $6\,^1\Sigma_g^+$ potential in which the two wells remain separated. Figure 12 shows the $6\,^1\Sigma_g^+$ radiative lifetimes obtained from the full [Eq. (4)] calculation for $J = 1$ and $J = 31$, plotted as a function of their vibrational level. The large difference of approximately a factor of three between the $J = 1$ and $J = 31$ lifetimes for $v = 40$ and for $v = 100$ occurs due to a "switch" of the wavefunction, which is predominantly the outer well for the long lifetime value, $v = 40, J = 31$ and $v = 100$, $J = 1$, and is predominantly the inner well for the shorter
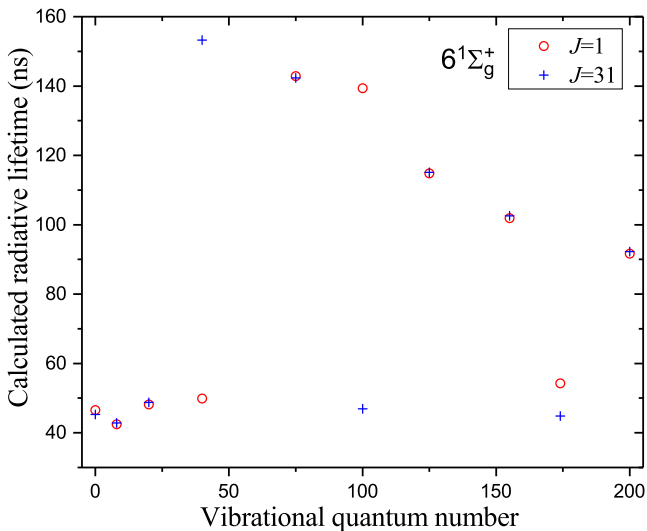

FIG. 12. Comparison of radiative lifetimes of J = 1 and J = 31 calculated for selected vibrational levels $v = 0, 8, 20, 40, 75, 100, 125, 155, 174$, and 200, using Eq. (4).

TABLE I. Calculated radiative lifetimes (in nanosecond) of selected ro-vibrational levels of the Na$_2$ $6\,^1\Sigma_g^+$ state.

v	$J = 1$	$J = 31$
0	46.4	45.3
7	42.5	42.8
8	42.5	42.9
20	48.2	48.8
40	49.9	153.2
75	142.9	142.4
100	139.4	46.9
125	114.8	115.1
155	101.9	102.6
174	54.3	44.9
200	91.7	92.3

lifetime value, $v = 40$, $J = 1$ and $v = 100$, $J = 31$. The results of these calculated radiative lifetimes are presented in Table I.

V. RESULTS AND DISCUSSION

A time-resolved double resonance spectroscopy technique has been applied to the sodium diatomic molecules in a heat-pipe, and the radiative lifetime of the $6\,^1\Sigma_g^+(7, 31)$ state was measured using a time-correlated photon counting technique. Also, lifetime calculations in various ro-vibrational levels of the $6\,^1\Sigma_g^+$ state using bound-bound and bound-free transitions were performed.

The radiative lifetimes are measured and the effect of argon gas collisions is eliminated with the Stern-Volmer extrapolation, explained in Sec. III. The measured radiative lifetime (extracted from the zero-pressure of the extrapolation) of the $6\,^1\Sigma_g^+$ (7, 31) state is found to be 39.56 ($\pm$2.23) ns, and our calculations showed that this value is 42.8 ns. Experimental and calculated radiative lifetimes reported in this work have been compared, and the results were in reasonable agreement. To validate our measurements and the techniques, we also measured the radiative lifetime of the $A\,^1\Sigma_u^+(8, 30)$ state by extrapolating the Stern-Volmer plot to zero pressure. The result is in good agreement with the literature values within the experimental uncertainties.

The observation of the non-linear behavior on the lifetimes at high pressures in the range of 500 mTorr–1800 mTorr may be due to the quenching effect. Further experimental and theoretical studies of the high pressure effect on the lifetime will be investigated in the future work. For the purpose of determining the radiative lifetime at the collision-free limit, a linear fit to the data was done at pressures below 500 mTorr. In addition, the observed dissociation signal from the Na 4p state does not originate from any resonance transition to the $6\,^1\Sigma_g^+$ (7, 31) state. The measured spectrum exists only when both lasers are turned on (see Fig. 3). Since the $6\,^1\Sigma_g^+$ (7, 31) state is about 2500 cm^{-1} below the (3s + 4p) asymptote collisional energy ($kT \approx 600$ cm^{-1}) is not sufficient to transfer $6\,^1\Sigma_g^+$ (7, 31) molecules into this asymptote. In addition, the dissociation signal appears only when molecules are formed in the heat-pipe ($\sim$280 °C), indicating that no atomic transitions exist with either laser. As a result, the observed dissociation signal has no effect on the measured lifetime. A possible channel for the dissociating molecule into the (3s + 4p) asymptote may be through a one-color two-photon transition. The information about the origin of observed dissociation can be studied in detail in a separate study and will not be detailed here.

TABLE II. Comparison of measured and calculated radiative lifetimes of the selected ro-vibrational levels of the Na$_2$ $6\,^1\Sigma_g^+$. Theoretical calculations are compared according to the bound-bound, denoted as bb, and bound-free, denoted as bf, transitions.

Method	Level	τ (ns)	Reference
Experiment	$6\,^1\Sigma_g^+(7, 31)$	39.56 ($\pm$2.23)	This work
Theory (bb + bf)	$6\,^1\Sigma_g^+(7, 31)$	42.8	This work
Theory (bb + bf)	$6\,^1\Sigma_g^+(7, 1)$	42.5	This work
Theory (bb)	$6\,^1\Sigma_g^+(7, 1)$	131	15

Table II is the tabulated outline of the measurements and theoretical calculations. A reasonable agreement between the experimental and theoretical results is achieved when bound-bound and bound-free transitions are considered.

VI. CONCLUSION

For the first time, experimental lifetime measurement of the $6\,^1\Sigma_g^+(7, 31)$ inner well and theoretical calculations in various ro-vibrational levels of the $6\,^1\Sigma_g^+$ state using bound-bound and bound-free transitions was performed. In addition, the effect of inclusion of the bound-free transitions in the calculated radiative lifetime of the $6\,^1\Sigma_g^+$ (3s + 5s) ro-vibrational levels in the range of $v = 0$–200 with $J = 1$ and $J = 31$ was reported. The results reveal the importance of the bound-free transitions and the rotational quantum number (e.g., a large difference of about a factor of three between the $J = 1$ and $J = 31$ for the $v = 40$ and $v = 100$, respectively) on the lifetime calculations. Also, the transition dipole moment functions coupling the $6\,^1\Sigma_g^+$ state to seven singlet, ungerade states and also the branching ratios for radiative transitions from the $6\,^1\Sigma_g^+$ ro-vibrational levels into those seven states were demonstrated. The measured and calculated radiative lifetimes are found to be 39.56 ($\pm$2.23) ns and 42.8 ns, respectively. The results are in reasonable agreement.

[1]W. C. Stwalley, Contemp. Phys. **19**, 65 (1978).
[2]W. C. Stwalley and H. Wang, J. Mol. Spectrosc. **195**, 194 (1999).
[3]K. M. Jones, P. D. L. E. Tiesinga, and P. S. Julienne, Rev. Mod. Phys. **78**, 483 (2006).
[4]L. D. Carr, D. DeMille, R. V. Krems, and J. Ye, New J. Phys. **11**, 055049 (2009).
[5]J. T. Bahns, P. L. Gould, and W. C. Stwalley, Mol. Opt. Phys. **42**, 171 (2000).
[6]B. McGuyer, M. McDonald, G. Iwate, M. Tarallo, W. Skomorowski, R. Moszynski, and T. Zelevinsky, Nat. Phys. **11**, 32 (2015).
[7]N. Balakrishnan, J. Chem. Phys. **145**, 150901 (2016).
[8]R. V. Krems, Phys. Chem. Chem. Phys. **10**, 4079 (2008).
[9]W. Demtröder, W. Stetzenbach, M. Stock, and J. Witt, J. Mol. Spectrosc. **61**, 382 (1976).
[10]T. W. Ducas, M. G. Littman, M. L. Zimmerman, and D. Kleppner, J. Chem. Phys. **65**, 842 (1976).
[11]G. Baumgartner, H. Kornmeier, and W. Preuss, Chem. Phys. Lett. **107**, 13 (1984).
[12]C. Radzewick, P. Kowalczyk, and J. Krasinski, Opt. Commun. **44**, 139 (1983).
[13]S. Magnier, P. Millié, O. Dulieu, and F. Masnou-Seeuws, J. Chem. Phys. **98**, 7113 (1993).
[14]C. C. Tsai, J. T. Bahns, and W. C. Stwalley, J. Mol. Spectrosc. **167**, 429 (1994).
[15]A. Sanli, B. Beser, J. R. Edwardson, S. Magnier, E. H. Ahmed, and A. M. Marjatta, J. Chem. Phys. **143**, 104304 (2015).
[16]R. B. Anunciado, S. Ashman, and L. Hüwel, J. Chem. Phys. **145**, 174306 (2016).

[17] T. Laue, P. Pellegrini, O. Dulieu, C. Samuelis, H. Knöckel, F. Masnou-Seeuws, and E. Tiemann, Eur. Phys. J. D **26**, 173 (2003).

[18] C. R. Vidal and J. Cooper, J. Appl. Phys. **40**, 3370 (1969).

[19] C. R. Vidal and F. B. Haller, Rev. Sci. Instrum. **42**, 1779 (1971).

[20] C. R. Vidal and M. M. Hessel, J. Appl. Phys. **43**, 2776 (1972).

[21] B. Steffes, X. Li, A. Mellinger, and C. R. Vidal, Appl. Phys. B **62**, 87 (1996).

[22] A. N. Nesmeyanov, *Vapor Pressure of the Elements* (Academic Press, New York, 1963).

[23] M. G. Littman and H. J. Metcalf, Appl. Opt. **17**, 2224 (1978).

[24] S. J. Seltzera and M. V. Romalis, J. Appl. Phys. **106**, 114905 (2009).

[25] R. Le Roy, "LEVEL 8.2: A computer program for solving the radial Schrödinger equation for bound and quasibound levels," Chemical Physics Research Report CP-663, University of Waterloo, 2014.

[26] S. Magnier, private communication (2017).

[27] E. Tiemann, H. Knöckel, and H. Richling, Z. Phys. D: At., Mol. Clusters **37**, 323 (1996).

[28] J. Camacho, A. Pardo, and J. Poyato, J. Phys. B **38**, 1935 (2005).

[29] E. Tiemann, Z. Phys. D: At., Mol. Clusters **5**, 77 (1987).

[30] A. Pashov, W. Jastrzebski, W. Jasniecki, V. Bednarska, and P. Kowalczyk, J. Mol. Spectrosc. **203**, 264 (2000).

[31] A. Grochola, W. Jastrzebski, and P. Kowalczyk, J. Mol. Spectrosc. **232**, 291 (2005).

[32] A. Sanli and M. Lyyra, private communication, Temple University (2018).

[33] A. Grochola, W. Jastrzebski, and P. Kowalczyk, Mol. Phys. **104**, 2569 (2006).

[34] A. Grochola, P. Kowalczyk, W. Jastrzebski, and A. Pashov, J. Chem. Phys. **121**, 5754 (2004).

[35] G. Herzberg, *Molecular Spectra and Molecular Structure. I. Spectra of Diatomic Molecules*, 2nd ed. (Van Nostrand Reinhold Company, New Jersey, 1950).

[36] P. F. Bernath, *Spectra of Atoms and Molecules*, 3rd ed. (Oxford University Press, Oxford, 2016).

[37] R. Le Roy and G. Kraemer, "BCONT 2.2: A computer program for calculating bound-continuum transition intensities for diatomic molecules," Chemical Physics Research Report CP-650R, University of Waterloo, 2004.

[38] B. McGeehan, Ph.D. thesis, Lehigh University, 2010.